Electronic structure and 4f-electron character in Ce$_2$PdIn$_8$ studied by angle-resolved photoemission spectroscopy

Q. Yao,[1,2] D. Kaczorowski,[3,4] P. Swatek,[3,5,6] D. Gnida,[3] C. H. P. Wen,[1] X. H. Niu,[1] R. Peng,[1] H. C. Xu,[1] P. Dudin,[7]
S. Kirchner,[8] Q. Y. Chen,[9,*] D. W. Shen,[2,10,†] and D. L. Feng[1,11]

[1]*State Key Laboratory of Surface Physics, Department of Physics, and Laboratory of Advanced Materials,*
Fudan University, Shanghai 200438, China
[2]*State Key Laboratory of Functional Materials for Informatics, Shanghai Institute of Microsystem and Information Technology (SIMIT),*
Chinese Academy of Sciences, Shanghai 200050, China
[3]*Institute of Low Temperature and Structure Research, Polish Academy of Sciences, P.O. Box 1410, 50-950 Wroclaw, Poland*
[4]*Centre for Advanced Materials and Smart Structures, Polish Academy of Sciences, Okolna 2, 50-422 Wroclaw, Poland*
[5]*Division of Materials Science and Engineering, Ames Laboratory, Ames, Iowa 50011, USA*
[6]*Department of Physics and Astronomy, Iowa State University, Ames, Iowa 50011, USA*
[7]*Diamond Light Source, Harwell Science and Innovation Campus, Didcot OX11 0DE, United Kingdom*
[8]*Zhejiang Institute of Modern Physics, Zhejiang University, Hangzhou, Zhejiang 310027, China*
[9]*Science and Technology on Surface Physics and Chemistry Laboratory, Mianyang 621908, China*
[10]*CAS Center for Excellence in Superconducting Electronics (CENSE), Shanghai 200050, China*
[11]*Collaborative Innovation Center of Advanced Microstructures, Nanjing 210093, China*

The localized-to-itinerant transition of f electrons lies at the heart of heavy-fermion physics, but has only been directly observed in single-layer Ce-based materials. Here, we report a comprehensive study on the electronic structure and nature of the Ce 4f electrons in the heavy-fermion superconductor Ce$_2$PdIn$_8$, a typical $n = 2$ Ce$_n$M$_m$In$_{3n+2m}$ compound, using high-resolution and 4d-4f resonant photoemission spectroscopies. The electronic structure of this material has been studied over a wide temperature range, and hybridization between f and conduction electrons can be clearly observed to form a Kondo resonance near the Fermi level at low temperatures. The characteristic temperature of the localized-to-itinerant transition is around 120 K, which is much higher than its coherence temperature $T_{coh} \sim 30$ K.

In heavy-fermion materials, f electrons generally exhibit both itinerant and localized features as the temperature changes. According to the standard Kondo lattice model, f electrons are localized at high temperatures, while conduction electrons would screen the local moments of f electrons to form Kondo singlets upon cooling, eventually resulting in an itinerant heavy Fermi-liquid ground state [1]. On the other hand, the recent two-fluid theory suggests that part of an atom's f electrons gives rise to the itinerant properties at low temperatures, while others account for the localization behavior at higher temperatures [2–5]. Experimentally, a detailed evolution of the localized-to-itinerant transition has also been hotly debated [6–10]. Recently, the hybridization between f and conduction electrons was extensively studied, and direct evidence for such a localized-to-itinerant transition has been observed in the CeMIn$_5$ family ($M = $ Co, Rh, Ir) [10–14]. However, in other Ce-based heavy-fermion compounds, the temperature evolution of the localized-to-itinerant transition of the f electrons still needs to be reported [15,16].

The Ce$_n$$MIn_{3n+2}$ ($M = $ Co, Rh, or Ir, with $n = 1$, 2, ∞) heavy-fermion compounds consist of n layers of CeIn$_3$, stacked sequentially along the c axis with one intervening layer of MIn$_2$ [17]. The electronic structure of the $n = \infty$ and 1 compounds, CeIn$_3$ and CeMIn$_5$, has been extensively studied by angle-resolved photoemission spectroscopy (ARPES) [10–12,18,19], which has been proved to be a powerful tool to directly observe the behavior of f electrons. For the $n = 2$ compounds, Ce$_2$CoIn$_8$ and Ce$_2$RhIn$_8$ have been investigated through off-resonant ARPES, and Ce 4f electrons were found to be predominantly localized in both compounds [15,16]. However, to date, reports on these $n = 2$ compounds by means of on-resonance ARPES are still needed, in which the use of the 4d-4f resonance would largely enhance the f-electron photoemission matrix element. Moreover, for another important $n = 2$ member, Ce$_2$PdIn$_8$ with the unique paramagnetic ground state, de Haas–van Alphen (dHvA) measurements [20] and x-ray photoelectron spectroscopy (XPS) [21] both suggest a delocalized character of the Ce 4f states therein, yet a direct observation of the f-electron behavior, and particularly the itinerant-to-localized transition, in this compound is still lacking.

In this Rapid Communication, we present a systematic ARPES study on Ce$_2$PdIn$_8$. Its electronic structure is comprehensively revealed and directly compared with first-principles calculations. In particular, the character of the f electrons is studied by resonant ARPES, and the localized-to-itinerant

*sheqiuyun@126.com
†dwshen@mail.sim.ac.cn
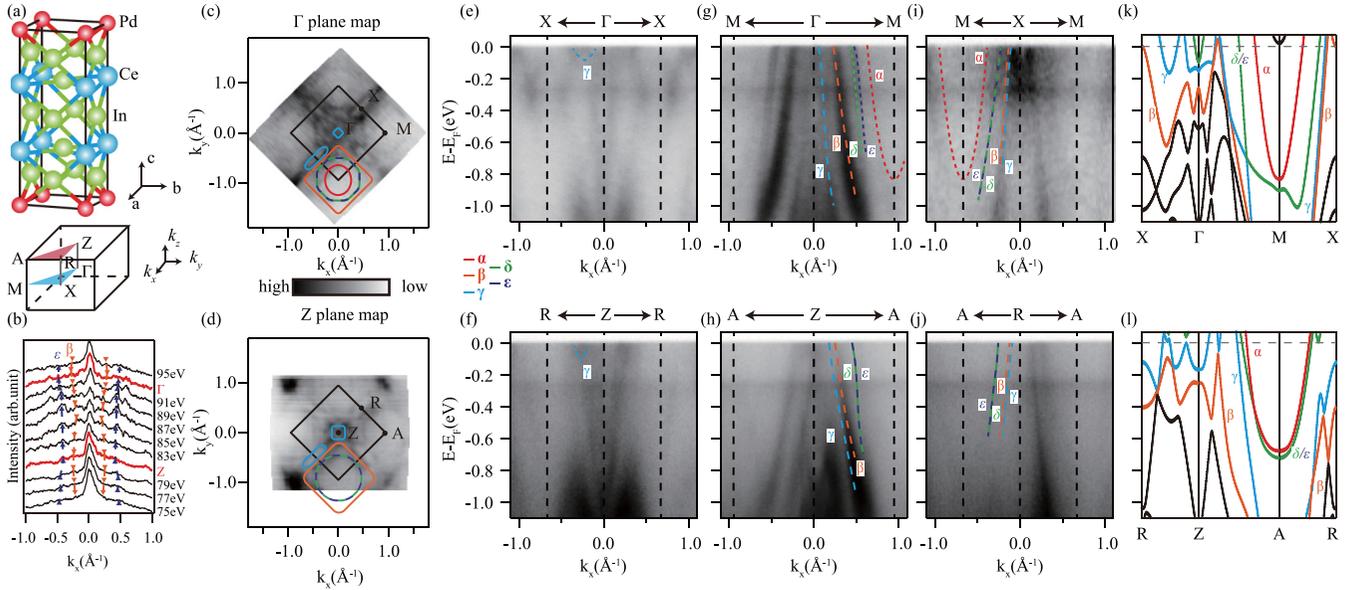
FIG. 1. (a) Crystal structure and the three-dimensional Brillouin zone of tetragonal Ce_2PdIn_8. (b) Momentum distribution curves taken with 75–95 eV photons along M-Γ-M. (c), (d) Photoemission intensity Γ and Z maps of Ce_2PdIn_8 at E_F, taken with 80- and 93-eV photon energies, respectively. The intensity was integrated over ($E_F - 10$ meV, $E_F + 10$ meV). (e), (g), and (i) Photoemission intensity plots along the M-Γ-M, X-Γ-X, and M-X-M directions. (f), (h), and (j) Photoemission intensity plots along the A-Z-A, R-Z-R, and A-R-A directions, respectively. (k), (l) Calculated bands along high-symmetry directions, which have been shifted upwards by $\sim$150 meV to match the experimental results.

transition is directly found to set in at a surprisingly high temperature.

High-quality single crystals of Ce_2PdIn_8 were synthesized by a self-flux method as described in Ref. [22]. ARPES measurements were conducted with photons from Beamline I05 of the Diamond Light Source, which is equipped with a Scienta R4000 electron analyzer. The overall energy resolution is 15–25 meV depending on the photon energy, and the angular resolution was set to 0.3°. Samples were cleaved at 10 K and then measured between 10 and 190 K under a vacuum better than 5×10^{-11} Torr. Electronic band-structure calculations of Ce_2PdIn_8 were performed with the all-electron general potential linearized augmented plane-wave (FL-APW) method as implemented in the WIEN2K code [23]. The exchange and correlation effects were treated using generalized gradient approximation (GGA) in the form proposed by Perdew, Burke, and Ernzerhof [24]. The Ce 2f electrons were removed from valence band as it was previously done in density functional theory (DFT) calculations for Ce_2RhIn_8 [12,16]. Spin-orbit coupling (SOC) was included as a second variational step with a basis of scalar-relativistic eigenfunctions, after the initial calculation was converged to self-consistency. The Monkhorst-Pack [25] special k-point scheme with $23 \times 23 \times 9$ mesh was used, resulting in 390 k points in the irreducible part of the Brillouin zone. The wave functions in the interstitial region were expanded using plane waves with a cutoff of $(R_{MT}K_{max}) = 8$, where K_{max} is the plane-wave cutoff, and R_{MT} is the smallest of all atomic sphere radii. Experimental lattice parameters have been used with atoms fixed in their bulk positions.

Figure 1(a) illustrates the crystal structure of Ce_2PdIn_8 and the corresponding three-dimensional Brillouin zone (BZ). This compound forms in the tetragonal Ho_2CoIn_8-type crystal

structure ($P4/mmm$) with lattice parameters $a = b = 4.69$ Å and $c = 12.185$ Å, and consists of a sequence of two $CeIn_3$ layers alternating with a $PdIn_2$ layer along the c axis [26]. To investigate its three-dimensional electronic structure, we have performed detailed k_z-dependent measurements by varying the photon energy between 75 and 95 eV. As shown in Fig. 1(b), there exists a weak photon-energy dependence of peak positions in the momentum distribution curves (MDCs) taken along the high-symmetry Γ-M direction, indicating the quasi-two-dimensional character. An inner potential of 13 eV, comparable to that of $CeIn_3$ [19], has been obtained through the best fit to the periodic variation of the MDCs' peak positions according to the free-electron final-state model [27], allowing us to determine the photon energies corresponding to the high-symmetry planes.

Figures 1(c) and 1(d) compare photoemission intensity maps for the ΓXM and ZAR planes, and their detailed photoemission intensity plots along high-symmetry directions are illustrated in Figs. 1(e)–1(j) using the same colors. The Fermi surfaces in the ΓXM plane consist of a square Fermi pocket around Γ and a racetrack pocket centered at X (both formed by the holelike band γ), and four pockets around M resulting from the Fermi crossings of the electronlike bands α, nearly degenerate ε/δ, and β. In the ZAR plane, both the shape of most Fermi pockets and the corresponding band dispersions exhibit only minor variations, confirming the quasi-two-dimensional character of these bands. Still, differences can be resolved between the Fermi-surface topologies of these two k_z planes. Changes in both the shape and size of the γ pocket in the ZAR plane imply a three-dimensional character of this band. The main bands in the vicinity of the Fermi level (E_F) have a similar orbital character to those in the $n = 1$ compound $CeCoIn_5$, while band splitting due to
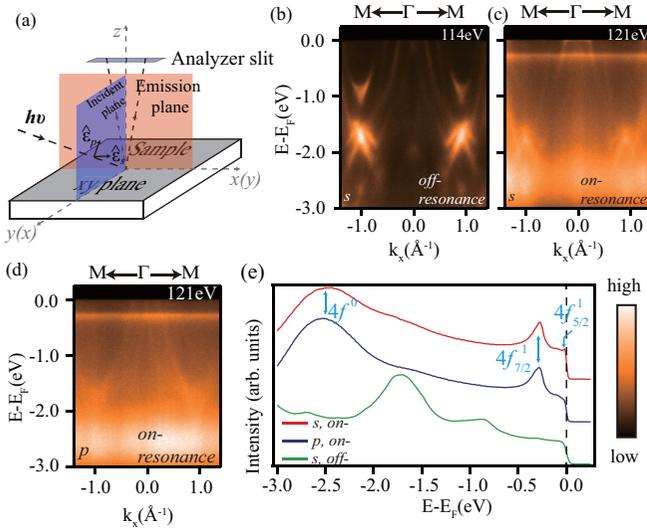
FIG. 2. (a) Experimental geometry for polarization-dependent ARPES. The emission plane is defined by the analyzer slit and the sample surface normal. p- and s-polarized light have polarization in and out of the emission plane, respectively. (b), (c) Photoemission intensity plots along M-Γ-M, taken with off-resonance (114 eV) and on-resonance (121 eV) s-polarized light, respectively. (d) On-resonance (121 eV) photoemission intensity plot along M-Γ-M, using p-polarized light. (e) Angle-integrated energy distribution curves (EDCs) of (b)–(d). Data were taken at 11 K.

interlayer coupling makes the band structure of Ce$_2$PdIn$_8$ more complex. Overall, our experimental data show a qualitative agreement with first-principles calculations, as displayed in Figs. 1(k) and 1(l).

In order to highlight the f-electron behavior, we chose 121-eV photons (the energy of the Ce 4d-4f transition) to realize a resonant enhancement of the Ce 4f photoionization

cross section. Figures 2(b) and 2(c) show the off-resonance and on-resonance photoemission intensity plots along Γ-M, taken with 114- and 121-eV photons, respectively, using s-polarized light. The corresponding on-resonance photoemission intensity plot taken with p-polarized light is displayed in Fig. 2(d). Here, p- and s-polarized light is defined to be from electric fields in and out of the emission plane, which is determined by the analyzer slit and the sample surface normal, as illustrated in Fig. 2(a).

As shown in Fig. 2(b), Pd 4d and Ce 5d states dominate the off-resonance spectra, consistent with the data shown in Fig. 1(e). The Ce 4f character is strongly enhanced in the on-resonance cases, as demonstrated by the flat bands in the photoemission intensity plots [Figs. 2(c) and 2(d)] and the apparent peaks in the corresponding integrated spectra [Fig. 2(e)]. The three evident features located around E_F, -0.25 and -2.5 eV below E_F, can be well understood by the single impurity Anderson model (SIAM) and were thus assigned as $4f_{5/2}^1$, $4f_{7/2}^1$, and $4f^0$, respectively [10,29]. Moreover, we note that the 4f state near E_F shows a sharp peak under s-polarized light but a broad hump in p-polarized light, and the overall f-electron intensity observed with p-polarized light is weaker than with s-polarized light. Therefore, further investigations of the Ce 4f states in this compound were performed with s-polarized light.

Next, we performed temperature-dependent ARPES measurements on this compound to investigate the evolution of the itinerant/localized nature of the f electrons with temperature. At 5 K, a flat f-electron feature near E_F can be clearly observed in the intensity plot, as demonstrated in Fig. 3(a). At this temperature, large f spectral weight can be clearly observed near E_F, suggesting a rather itinerant nature of the f electrons. Upon increasing the temperature, the spectral weight of the f states gradually diminishes while that of the β band is still preserved even to a rather high temperature (180 K). This temperature dependence is also clearly visible
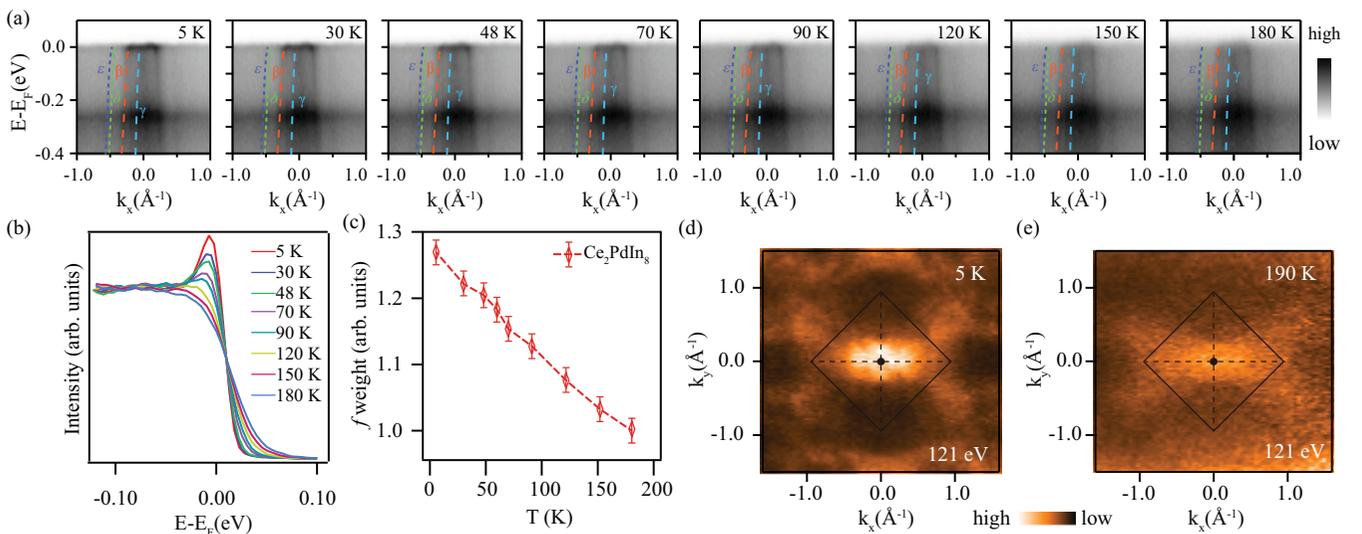
FIG. 3. Temperature evolution of the electronic structure of Ce$_2$PdIn$_8$. (a) Resonant (121 eV) photoemission intensities along the M-Γ-M direction at different temperatures as labeled, in which the dispersions of the conduction bands were extracted by MDC analysis (see Supplemental Material [28]). (b) Temperature dependence of EDCs around Γ. (c) Temperature-dependent quasiparticle spectral weight in the vicinity of Γ near E_F for Ce$_2$PdIn$_8$. (d), (e) Photoemission maps taken at 5 and 190 K, respectively.
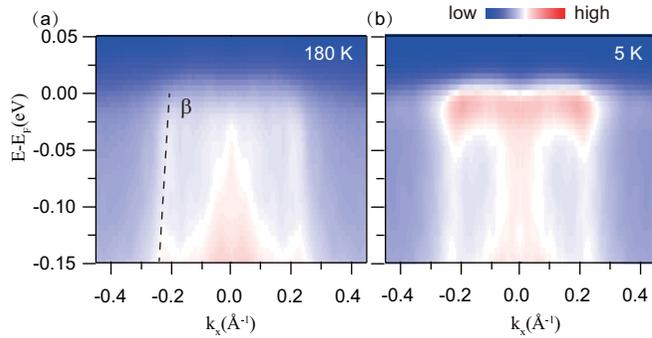
FIG. 4. Comparison of the photoemission intensity plot between high and low temperature in Ce$_2$PdIn$_8$. (a) Zoomed-in ARPES data along the Γ-M direction taken at 180 K. (b) Same as (a), but taken at 5 K.

FIG. 5. Development of the heavy quasiparticle band in Ce$_2$PdIn$_8$. (a) Photoemission intensity plot along Γ-M taken at 30 K, divided by the resolution-convoluted Fermi-Dirac distribution. The gray solid lines illustrate how the conduction β and γ bands hybridize with the f bands. The triangles and solid circles in colors are obtained by fitting individual MDCs and EDCs (see the Supplemental Material [28]). (b) EDCs corresponding to the spectrum in (a) in the momentum window $[-0.25$ Å^{-1}, 0.25 Å$^{-1}]$, showing a weakly dispersive feature.

when directly comparing the EDCs at Γ taken at different temperatures [Fig. 3(b)]. We observe a suppression of the f spectral weight upon increasing temperature, and the sharp f-electron quasiparticle peak near E_F is no longer visible at 150 K. Figure 3(c) presents the temperature dependence of f-electron spectral weight in the vicinity of Γ in Ce$_2$PdIn$_8$, which is obtained by integrating the EDCs over $[E_F - 100\text{meV}, E_F + 10 \text{ meV}]$. Here, the spectral weight has been normalized at 200 K and is found to keep rising with the decreasing temperature, showing the same trend as Fig. 3(b).

For comparison, Figs. 3(d) and 3(e) show the normalized photoemission intensity maps taken at 5 and 190 K, respectively. In the 5-K Fermi-surface map, the normalized intensity around the Brillouin zone center is strongly enhanced, originating from the itinerant f states. In contrast, the f electron spectral weight around the same momentum is greatly suppressed for the map contour taken at 190 K. Note that we have presented both maps using the same color scale, so the much higher spectral weight around the zone center at 5 K should not be artificial. Moreover, as shown in the Supplemental Material [28], a direct comparison of MDCs taken at 5 and 190 K can further confirm the spreading out of the f-band spectral weight from the zone center to somewhere with the increasing temperature. All the above data explicitly show the characteristic localized-to-itinerant crossover of f electrons. Remarkably, the occurrence of hybridization starts from about 120 K in Ce$_2$PdIn$_8$, which is much higher than $T_\text{coh} \sim 30$ K [22,30–32].

In Fig. 4 we present the zoomed-in photoemission intensity plot near E_F to concentrate on the f-electron character and quasiparticle bands. Compared with spectra taken at high temperatures, when the β band shows linear dispersion, evident bending of this band around E_F can be observed at the low temperature [Fig. 4(a)]. This is a direct evidence of the hybridization between the f and conduction electrons. According to the standard view on the heavy-fermion ground state based on the periodic Anderson model (PAM), the hybridization between the f and conduction electrons would create two separate bands with band bending near E_F. Meanwhile, the f spectral weight should be redistributed, with a significant enhancement to the "inside" of the holelike bands and the "outside" of the electronlike bands. In Fig. 4(b),

we indeed observe the enhancement of the f spectral weight "inside" of the holelike β band, which is more evidence for the hybridization between the f and conduction electrons in Ce$_2$PdIn$_8$. Such behavior is similar to that observed in the heavy-fermion compound CeIrIn$_5$ [14].

To further quantitatively investigate the hybridization of conduction bands and f electrons, we zoomed in on the spectral feature around Γ in the vicinity of E_F and then performed the PAM fitting, which has been proved to be an effective way to study the f-electron behaviors [10,13]. Details of the band dispersion extraction and the PAM fitting can be found in the Supplemental Material [28]. Here, the resolution-convoluted Fermi-Dirac distribution has been divided in order to probe the band structure slightly above E_F, as shown in Fig. 5(a).

Quantitatively, a fit to the PAM picture gives a renormalized hybridization $V_k = 15 \pm 5$ meV for both conduction bands, which implies the substantial hybridization strength between f electrons and conduction d bands. Moreover, as shown in Fig. 5(b), a heavy quasiparticle band is induced with an energy dispersion of around 6 meV, which is larger than that in CeIn$_3$ [18,33], indicating a stronger hybridization in CeIn$_3$.

To summarize, we have characterized the electronic structure and f-electron behavior of Ce$_2$PdIn$_8$ using high-resolution resonant and nonresonant ARPES. Besides presenting the low-lying electronic structure of this material, we have shown how localized f electrons in Ce$_2$PdIn$_8$ become partially itinerant and evolve into the heavy-fermion state from a much higher temperature than the coherence temperature T_coh. These findings provide a comprehensive experimental picture of the character of f electrons in Ce$_2$PdIn$_8$, complementing our understanding of the f electrons' itinerant-to-localized evolution in the Ce$_n$M$_m$In$_{3n+2m}$ heavy-fermion family.

---

[1] P. Coleman and A. H. Nevidomskyy, J. Low Temp. Phys. **161**, 182 (2010).

[2] Y. F. Yang, Z. Fisk, H.-O. Lee, J. D. Thompson, and D. Pines, Nature (London) **454**, 611 (2008).

[3] Y. F. Yang and D. Pines, Phys. Rev. Lett. **100**, 096404 (2008).

[4] Y. F. Yang and D. Pines, Proc. Natl. Acad. Sci. USA **109**, E3060 (2012).

[5] Y.-F. Yang, R. Urbano, N. J. Curro, D. Pines, and E. D. Bauer, Phys. Rev. Lett. **103**, 197004 (2009).

[6] H. Shishido, R. Settai, D. Aoki, S. Ikeda, H. Nakawaki, N. Nakamura, T. Iizuka, Y. Inada, K. Sugiyama, T. Takeuchi, K. Kindo, T. C. Kobayashi, Y. Haga, H. Harima, Y. Aoki, T. Namiki, H. Sato, and Y. Ōmuki, J. Phys. Soc. Jpn. **71**, 162 (2002).

[7] K. Haule, C.-H. Yee, and K. Kim, Phys. Rev. B **81**, 195107 (2010).

[8] A. Koitzsch, S. V. Borisenko, D. Inosov, J. Geck, V. B. Zabolotnyy, H. Shiozawa, M. Knupfer, J. Fink, B. Büchner, E. D. Bauer, J. L. Sarrao, and R. Follath, Phys. Rev. B **77**, 155128 (2008).

[9] A. Koitzsch, I. Opahle, S. Elgazzar, S. V. Borisenko, J. Geck, V. B. Zabolotnyy, D. Inosov, H. Shiozawa, M. Richter, M. Knupfer, J. Fink, B. Büchner, E. D. Bauer, J. L. Sarrao, and R. Follath, Phys. Rev. B **79**, 075104 (2009).

[10] Q. Y. Chen, D. F. Xu, X. H. Niu, J. Jiang, R. Peng, H. C. Xu, C. H. P. Wen, Z. F. Ding, K. Huang, L. Shu, Y. J. Zhang, H. Lee, V. N. Strocov, M. Shi, F. Bisti, T. Schmitt, Y. B. Huang, P. Dudin, X. C. Lai, S. Kirchner, H. Q. Yuan, and D. L. Feng, Phys. Rev. B **96**, 045107 (2017).

[11] S.-i. Fujimori, T. Okane, J. Okamoto, K. Mamiya, Y. Muramatsu, A. Fujimori, H. Harima, D. Aoki, S. Ikeda, H. Shishido, Y. Tokiwa, Y. Haga, and Y. Ōnuki, Phys. Rev. B **67**, 144507 (2003).

[12] S.-i. Fujimori, A. Fujimori, K. Shimada, T. Narimura, K. Kobayashi, H. Namatame, M. Taniguchi, H. Harima, H. Shishido, S. Ikeda, D. Aoki, Y. Tokiwa, Y. Haga, and Y. Ōnuki, Phys. Rev. B **73**, 224517 (2006).

[13] Q. Y. Chen, D. F. Xu, X. H. Niu, R. Peng, H. C. Xu, C. H. P. Wen, X. Liu, L. Shu, S. Y. Tan, X. C. Lai, Y. J. Zhang, H. Lee, V. N. Strocov, F. Bisti, P. Dudin, J.-X. Zhu, H. Q. Yuan, S. Kirchner, and D. L. Feng, Phys. Rev. Lett. **120**, 066403 (2018).

[14] Q. Y. Chen, C. H. P. Wen, Q. Yao, K. Huang, Z. F. Ding, L. Shu, X. H. Niu, Y. Zhang, X. C. Lai, Y. B. Huang, G. B. Zhang, S. Kirchner, and D. L. Feng, Phys. Rev. B **97**, 075149 (2018).

[15] S. Raj, Y. Iida, S. Souma, T. Sato, T. Takahashi, H. Ding, S. Ohara, T. Hayakawa, G. F. Chen, I. Sakamoto, and H. Harima, Phys. Rev. B **71**, 224516 (2005).

[16] R. Jiang, D. Mou, C. Liu, X. Zhao, Y. Yao, H. Ryu, C. Petrovic, K.-M. Ho, and A. Kaminski, Phys. Rev. B **91**, 165101 (2015).

[17] W. Bao, P. G. Pagliuso, J. L. Sarrao, J. D. Thompson, Z. Fisk, and J. W. Lynn, Phys. Rev. B **64**, 020401 (2001).

[18] Y. Zhang, W. Feng, X. Lou, T. Yu, X. Zhu, S. Tan, B. Yuan, Y. Liu, H. Lu, D. Xie, Q. Liu, W. Zhang, X. Luo, Y. Huang, L. Luo, Z. Zhang, X. Lai, and Q. Chen, Phys. Rev. B **97**, 045128 (2018).

[19] Y. Zhang, H. Lu, X. Zhu, S. Tan, Q. Liu, Q. Chen, W. Feng, D. Xie, L. Luo, Y. Liu, H. Song, Z. Zhang, and X. Lai, Sci. Rep. **6**, 33613 (2016).

[20] K. Götze, J. Klotz, D. Gnida, H. Harima, D. Aoki, A. Demuer, S. Elgazzar, J. Wosnitza, D. Kaczorowski, and I. Sheikin, Phys. Rev. B **92**, 115141 (2015).

[21] M. Werwiński, A. Szajek, A. Ślebarski, and D. Kaczorowski, J. Alloys Compd. **647**, 605 (2015).

[22] D. Kaczorowski, A. P. Pikul, D. Gnida, and V. H. Tran, Phys. Rev. Lett. **103**, 027003 (2009).

[23] P. Blaha, K. Schwarz, G. K. H. Madsen, D. Kvasnicka, and J. Luitz, *WIEN2K, An Augmented Plane Wave + Local Orbitals Program for Calculating Crystal Properties* (Karlheinz Schwarz, Technische Universität Wien, Austria, 2001).

[24] J. P. Perdew, K. Burke, and M. Ernzerhof, Phys. Rev. Lett. **77**, 3865 (1996).

[25] H. J. Monkhorst and J. D. Pack, Phys. Rev. B **13**, 5188 (1976).

[26] A. Tursina, S. Nesterenko, Y. Seropegin, H. Noël, and D. Kaczorowski, J. Solid State Chem. **200**, 7 (2013).

[27] S. Hüfner, *Photoelectron Spectroscopy* (Springer, New York, 2003), pp. 39–60.

[28] See Supplemental Material at http://link.aps.org/supplemental/10.1103/PhysRevB.99.081107 for detailed band dispersion analyses.

[29] O. Gunnarsson and K. Schönhammer, Phys. Rev. B **28**, 4315 (1983).

[30] D. Kaczorowski, A. P. Pikul, D. Gnida, and V. H. Tran, Phys. Rev. Lett. **104**, 059702 (2010).

[31] D. Kaczorowski, A. Pikul, B. Belan, L. Sojka, and Y. Kalychak, Physica B **404**, 2975 (2009).

[32] D. Kaczorowski, D. Gnida, A. Pikul, and V. Tran, Solid State Commun. **150**, 411 (2010).

[33] S. Fujimori, J. Phys.: Condens. Matter **28**, 153002 (2016).